Available online at www.sciencedirect.com
ScienceDirect
Polymer 48 (2007) 5802–5812
polymer
www.elsevier.com/locate/polymer

Atomistic molecular simulations of structure and dynamics of crosslinked epoxy resin

Chaofu Wu, Weijian Xu*

Institute of Polymer Research, Department of Chemistry and Chemical Engineering, Hunan University, Changsha 410082, People's Republic of China

Received 4 March 2007; received in revised form 30 June 2007; accepted 6 July 2007
Available online 15 July 2007

Abstract

Many excellent thermal and mechanical performances of cured epoxy resin products can be related to their specific network structure. In this work, a typical crosslinked epoxy resin was investigated using detailed molecular dynamics (MD) simulations, in a wide temperature range from 250 K to 600 K. A general constant-*NPT* MD procedure widely used for linear polymers failed to identify the glass transition temperature (T_g) of this crosslinked polymer. This can be attributed to the bigger difference in the time scales and cooling rates between the experiments and simulations, and specially to the highly crosslinked infinite network feature. However, by adopting experimental densities appropriate for the corresponding temperatures, some important structural and dynamic features both below and above T_g were revealed using constant-*NVT* MD simulations. The polymer system exhibited more local structural features in case of below T_g than above T_g, as suggested by some typical radial distribution functions and torsion angle distributions. Non-bond energy, not any other energy components in the used COMPASS forcefield, played the most important role in glass transition. An abrupt change occurring in the vicinity of T_g was also observed in the plots of the mean squared displacements (MSDs) of the crosslinks against the temperature, indicating the great importance of crosslinks to glass transition. Rotational dynamics of some bonds in epoxy segments were also investigated, which exhibited great diversity along the chains between crosslinks. The reorientation functions of these bond vectors at higher temperatures can be well fitted by Kohlrausch–Williams–Watts (KWW) function.

Keywords: Crosslinked epoxy resin; Atomistic molecular simulations; Glass transition temperature

1. Introduction

Crosslinked epoxy resins, resulting from open-ring copolymerization of epoxy resins by "hardener" compounds, are a major class of thermosetting polymers, which exhibit many superior performances to the linear polymers, such as high modulus and fracture strength, low creep and high-temperature performances, etc. In general, these excellent performances can be attributed to their specific chemical structure compared to the linear polymers: highly crosslinked infinite network, without well-defined main or side chains, or appropriate polymer repeating units. The average weight between crosslinks M_c, the concentration of elastic chains υ, and the crosslink density n are thus the most important structural parameters, which have been empirically related to the shear and tensile modulus [1] and glass transition temperature (T_g) [2–4]. However, more detailed structural characterization is required to improve our understanding and even prediction of those properties or phenomena.

Despite extensive experiments and theories, many computer simulations have been carried out, primarily, including Monte Carlo (MC) simulations of network formation [5–7] and molecular dynamics (MD) simulations of network structure [8]. From the former, the complete topological structure and the distribution of the molecular weights can be obtained, which enable M_c, υ, n, gel points, number-average molecular weight M_n, and weight-average molecular weight M_w to be determined. From the latter, one can study the effects of

* Corresponding author. Tel./fax: +86 731 8821749
E-mail address: weijxu@hnu.cn (W. Xu).

0032-3861/$ - see front matter © 2007 Elsevier Ltd. All rights reserved.
doi:10.1016/j.polymer.2007.07.019

monomer connectivity on those mechanical and thermal properties. All these simulation methods represent a class of attractive tools for studying polymer networks because of the ability to provide control over the details of the network in a much simpler way than through experimentation [9]. Specifically, MD simulations allow one to study molecular mechanism of important chemical and physical processes and to quantify the effects of variables such as the strand length, extent of reaction, chain topology and functionality on the physical properties of the network. These simulations not only can test theoretical models but also can provide additional insight into experimentally observed behavior.

However, it should be noted that all those simulations described above have been on coarse-grained models, which completely or partially neglect the chemical details and interactions. In order to study a specific chemical system and some practical problems, an atomistic model must be employed. To this end, great complexity coupled with the added computational cost is expected in modeling the realistic polymer network. A relatively simple model was therefore developed by us [10] to reduce the impact of them. When appreciate forcefield (COMPASS) was used, molecular mechanics calculation based on this model was found to reproduce reasonable static properties (such as density and elastic constants). In this work, the detailed structure and dynamics of the polymer network chains were investigated by using MD simulation. The cases at various temperatures below and above T_g would be compared to each other, with a trial towards understanding the glass transition occurring in the polymer networks.

The characteristic temperature T_g is an important indication of heat resistance of the polymer materials [11], and it can also indicate molecular or ion mobility [12,13]. Moreover, T_g can help assess the interaction strength and miscibility of polymer blends [14]. Therefore, many experiments combined with theories were performed previously to understand the structure–T_g relationship [15–18]. Besides, a variety of atomistic simulation works were also devoted to this topic. However, these simulations were only carried out on linear polymers but none on such complex polymers as crosslinked epoxy resins, which would show very distinct physics and chemistry, has been discovered. It is worthwhile to point out that even the understanding of the glass transition occurring in any polymer is still far from complete, and this work only presents an initial study towards a more comprehensive one for the sake of relatively simpler model employed and current computational power.

2. Simulation procedure

The studied epoxy network system was based on diglycidyl ether bisphenol A (DGEBA) and isophorone diamine (IPD), whose important physical properties from the reference article [19] are shown in Table 1. The amorphous polymer model was dynamically built by making some reasonable assumptions. Firstly, 16 epoxy segments and 8 hardener segments containing reactive sites were packed into a 3D periodic cell box according to self-avoiding random-walk method of Theodorou and Suter. This formulation was then mixed by using molecular dynamics

Table 1
Summary of some important physical properties of the epoxy-amine copolymer network system based on DGEBA and IPD

Physical property	Value
Density ρ at 300 K, g cm^{-3}	1.131
Glass transition temperature T_g, K	436
Volume expansive coefficient α_{glassy}, 10^{-4} K^{-1}	2.46
Volume expansive coefficient $\alpha_{rubbery}$, 10^{-4} K^{-1}	5.96

The data were abstracted from Ref. [19].

(MD) after initial energy minimization (MM) based on a generic Dreiding2.21 forcefield. Under close proximity, covalent bonds were formed between the nearest reactive pairs within the reaction cutoff distance considering the removal of ring catenation or spearing. Repeating MM and MD to form bonds for several times, a crosslinked polymer network with a conversion of 93.7% was finally obtained for the following simulations. This procedure was described in detail in our previous paper [10]. The resulting model system has a cell dimension 21.55 Å × 21.55 Å × 21.55 Å, depicted in Fig. 1 in two different styles. In this model system, there are only two ''free'' (unreacted) hydroxyl groups and one ''free'' amine group with two hydrogen atoms. The chemical structures of the resin and hardener segments are also shown in Fig. 1.

After the initial microstructure was generated, the minimization of the potential energy of the model system was carried out, where a well-validated COMPASS forcefield [20] was used. Next, 100 ps constant-*NVT* MD simulation was performed at 600 K to relax the polymer chains, followed by 500 ps constant-*NPT* MD simulation to obtain optimized density. The system was then cooled stepwise to 250 K with the rate of 50 K/600 ps. At each temperature, a constant-*NVT* MD simulation of 100 ps and a constant-*NPT* MD simulation of 500 ps with time step 1 fs were carried out. It can be seen that the time-averaged densities at all temperatures tend to be in steady states at the latter stage. Finally, the resulting configurations with the experimental densities appropriate for the temperatures were used to initiate constant-*NVT* dynamics for a period of 2–3 ns. For higher temperatures (450–600 K), 2 ns constant-*NVT* dynamics was performed, whereas for lower temperatures (250–400 K), 3 ns constant-*NVT* dynamics was performed. This is due to the fact that the model system relaxes more slowly to equilibrium at the lower temperatures. In terms of non-bonding interaction treatments, separate methods were employed for the van der Waals interactions and Columbic interactions. For the former, atom-based direct cutoff of 9.5 Å and a buffer of 0.5 Å were used whereas for the latter Eward summation and CMM were employed for constant-*NVT* MD and constant-*NPT* MD simulations, respectively, depending on the accuracy and efficiency of the computation. Velocity Verlet algorithm with time step of 1 fs was used for the integration of the atom motion equations throughout all MD simulations. Andersen method [21] and Berendsen method [22] were adopted for controlling the temperature and pressure, respectively.

In this work, more realistic MD (constant-*NPT* MD and constant-*NVT* MD) simulations were employed for simulating

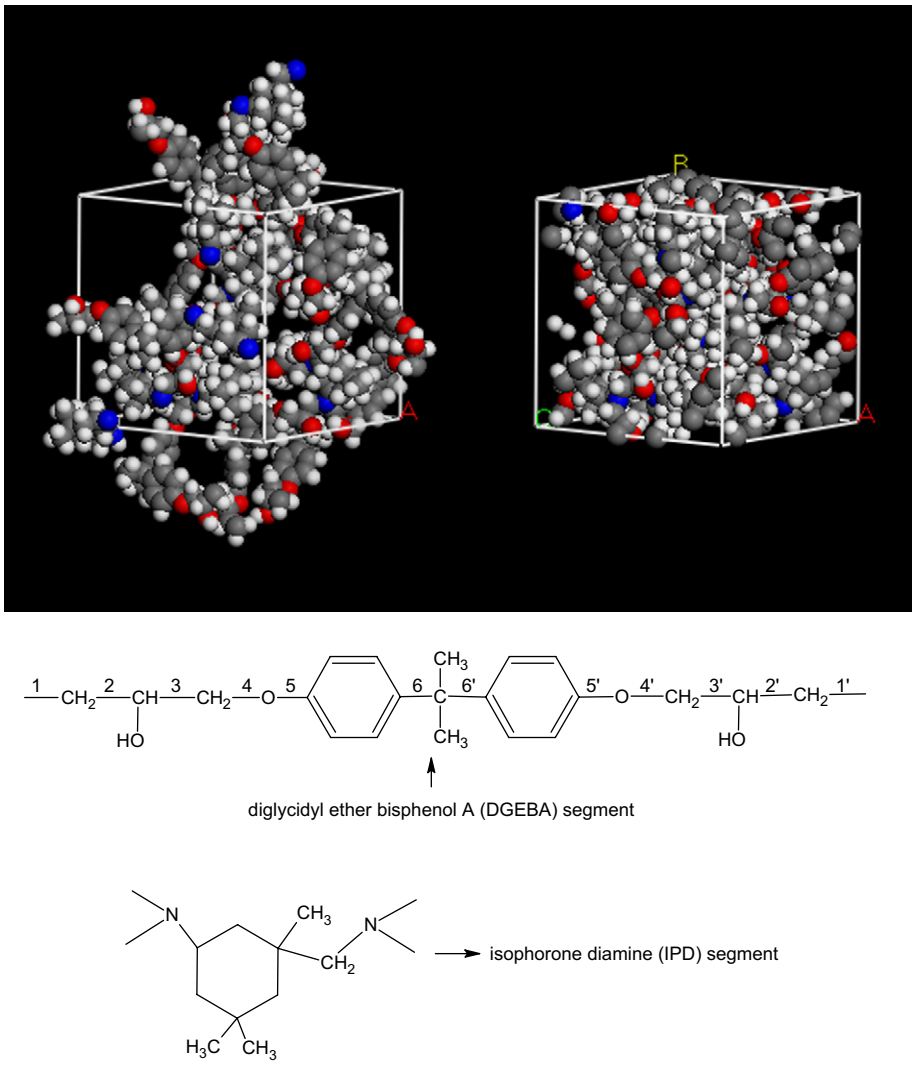

Fig. 1. System models of crosslinked epoxy-amine polymer network (top left: unit cell without periodic boundary; top right: same unit cell but with periodic boundary) and chemical structures of the two main monomer segments.

the motions of all atoms in the studied system over time under some appreciate thermodynamic conditions. The constant-*NPT* MD represented constant number of atoms or molecules, constant pressure, and constant temperature, which was primarily used to bring the systems into equilibrium suggested by energy and density stability. And the constant-*NVT* MD was performed at constant number of atoms or molecules, constant volume, and constant temperature for further equilibrating and collecting data for property analysis of structure, energy, and dynamics. Most simulations described above were performed using the Materials Studio 4.0 software [23].

3. Results and discussion

3.1. Consideration of the simulated model

Following the general procedure widely used for the linear polymers [24–27], a trial to identify the T_g from the V–T curve was firstly made. It can be noticed that the calculated density ρ at 300 K is 1.122 g cm^{-3}, which compares well with the corresponding experimental value 1.131 g cm^{-3} [19]. A steady decrease with temperature is observed in Fig. 2, but unfortunately, no distinctive changes mark the location of T_g. In fact, all eight V–T data can be well fitted as a straight line, from whose slope the volume expansive coefficient α_P at constant pressure P can be obtained according to

$$\alpha_P = \frac{1}{v_0}\left(\frac{\partial v}{\partial T}\right)_P \quad (1)$$

where v is the specific volume at temperature T and v_0 is the specific volume at a reference temperature such as 300 K. The calculated α_P is about 2.53×10^{-4} K^{-1}, which is very close to the experimental value 2.46×10^{-4} K^{-1} at the glassy region [19]. So all the densities below 450 K compare well with the corresponding experimental values. However, this constant-*NPT* MD procedure fails to reproduce the experimental α_P at rubbery region within the studied temperature range and thus fails to locate the volumetric T_g. One can speculate to

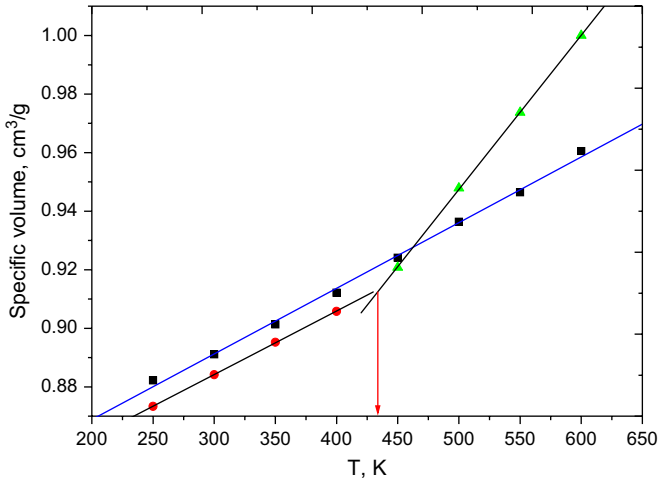

Fig. 2. Specific volume versus temperature of the DGEBA-IPD system obtained from this simulation work (green line fitting black dots) and inferred from the experimental data (black lines across red or blue dots), assuming linear relationship both below and above Tg. (For interpretation of the references to colour in this figure legend, the reader is referred to the web version of this article.)

obtain T_g from a wider temperature range, which would lead to the simulated T_g attaining up to above 600 K, much higher than the experimental value 436 K. As frequently discussed [28], on one hand, the limited time scale and fast cooling rate in the simulations were the cause of T_g elevation. On the other hand, the experimental T_g was frequency and cooling rate dependent [29,30]. Besides, the highly crosslinked infinite network can be responsible for this bigger difference. However, it should be noted that the stepwise polymerization following minimization can generate physically reasonable initial configuration. In order to model other structural and dynamic properties of the realistic crosslinked system both below and above T_g, the experimental densities at various temperatures were adopted. These experimental densities were determined from the density at about 300 K by assuming the linear relations between the specific volume and temperature at both the glassy and rubbery regions. This procedure is also schemed in Fig. 2, where the broken temperature of the two straight lines with different slopes is T_g, which is actually the reverse route to predict T_g and α_P as discussed above.

3.2. Static structure

3.2.1. Packing modes of the polymer networks

Firstly, the structural aspects of bulk amorphous melts of the epoxy-amine polymer were examined using radial distribution functions (RDFs) [31]. Calculated RDFs at two typical temperatures 300 K and 600 K are shown in Fig. 3(a) for this bulk system. All atoms and the last 1000 configurations from constant-*NVT* MD simulations were included in these calculations. Common features are demonstrated for the two different temperatures. The absence of any RDF at the distance less than 0.9 Å is due to the excluding volume effects. The first peak at around 1.1 Å corresponds to the bond

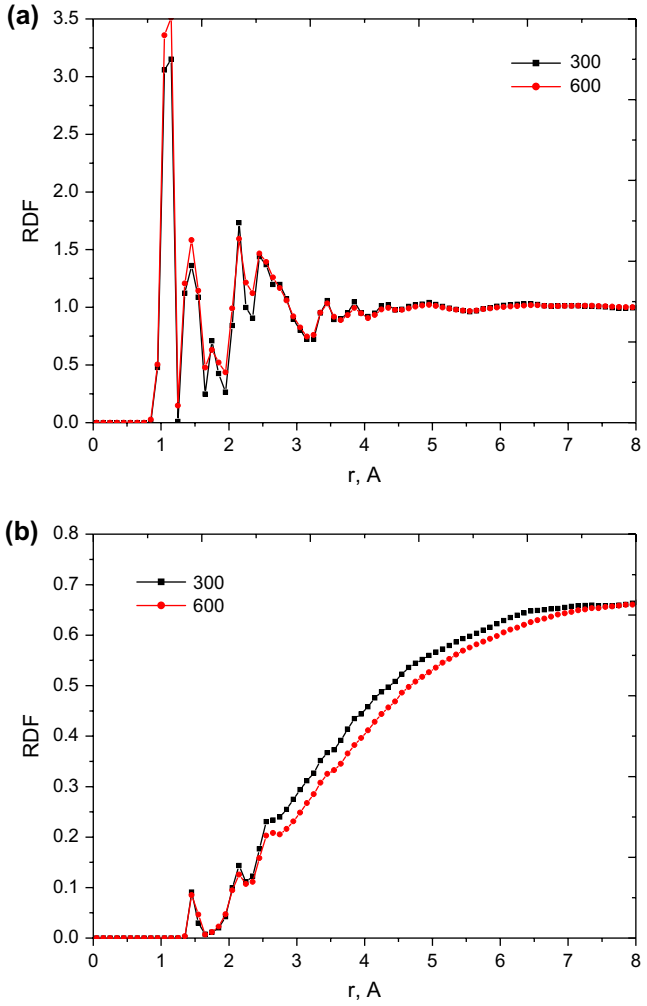

Fig. 3. Total radial distribution functions (RDFs) (a) and the intermolecular contributions (b) for all the atoms involved in the cured epoxy system at the two typical temperatures 300 K and 600 K.

distance between hydrogen and other atoms. The second peak at around 1.45 Å comes from the bond distance between carbon and non-hydrogen atoms. The third peak at around 1.75 Å is attributed to the distance between the two hydrogen atoms (H–C–H) in the methyl group. The subsequent intramolecular peaks result from distances between atoms two bonds apart, such as hydrogen and carbon in H–C–C sequences (~2.16 Å), carbon atoms in C–C–C sequences (~2.44 Å) [32]. Among these peaks, the atom pairs associated with polar atoms are not expected to exhibit an important contribution because of the much lower fraction. Other peaks up to 4 Å are of intramolecular origin and reflect mainly relative positions and interactions between non-bond atoms separated by more than three bonds. Note that any sharp peaks at distances greater than 4 Å are absent and the RDFs tend to 1, which is generally regarded as the proof of the amorphous nature of the polymer system [33]. The intermolecular contributions to the total RDFs, shown in Fig. 3(b), provide another proof in that no sharp peaks are observed in this distance range, which is consistent with the absence of crystalline-like order. The presence of some small sharp peaks at distance

less than 4 Å is due to the artificial treatments of constructing the model, i.e. some chemical bonds in the central cell cross-over the periodic boundary with those in the image cells. As far as the temperature dependence is concerned, the total RDFs only exhibit slight variations in the height of the first and second peaks: the RDF at 600 K is slightly higher than that at 300 K. As depicted in Fig. 3(b), the intermolecular RDF at 600 K is slightly lower than that at 300 K, which reveals the change in density of the polymer system.

For the epoxy systems containing hydroxyl and amine groups, there would be great possibility for hydrogen bonding, which is very important to glass transition. Actually, the H-bonding interactions have been attempted to estimate T_g of a linear epoxy system [34]. In that work, a simple forcefield Dreiding2.21 was used to directly calculate hydrogen bonding interaction energies. Since the forcefield COMPASS was used, where hydrogen bonding interactions were implicitly considered, this method is not applicable to our system. On the contrary, we examined these interactions by comparing RDFs of polar atom pairs at the two different temperatures (300 K and 600 K). The presence of three classes of hydrogen bonds (H-bonds) in this studied system was confirmed: hydroxyl–hydroxyl, hydroxyl–ether, and hydroxyl–nitrogen, as shown in Fig. 4. It can be seen that the sharp peaks associated with regular (2.75 Å) and twist (3.15 Å) H-bonds at 600 K are generally lower in intensity than those at 300 K, indicating that the H-bonds decrease with increasing temperature as expected. Moreover, the three RDFs exhibit more structural features at lower temperature than at higher temperature. Specially, at distances greater than 4 Å, some broad peaks are observed at 300 K whereas these broad peaks at the same distance are reduced or smoothed at 600 K because of the superposition. Similar phenomena have been observed by Bennemann and coworkers [35].

3.2.2. Interaction energies and torsion distributions

Various interaction energies can also be used to analyze glass transition occurring in the polymer systems. On this point, Soldera [36] has performed energetic analysis of the two PMMA chain tacticities on glass transition. Before this work, he [37] reported a break in the plots of total, intramolecular, and intermolecular potential energies versus temperature of this PMMA system near T_g. Fried and Ren [24] also found a break in the plots of internal energy versus temperature of PuBuP system in the vicinity of T_g. In fact, for our simulations, it is more convenient to analyze the roles of energy components in glass transition. The simulated results of bond energy, angle energy, torsion energy, and non-bond energy against the temperature are plotted in Fig. 5. It can be seen that only in the plot of non-bond energy versus temperature is there a break present, indicating the occurrence of glass transition. At both below and above T_g, non-bond energy increases almost linearly with increasing temperature with a break at T_g. But for the other energy components, they consistently increase almost linearly with increasing temperature in the whole temperature range. These results show that the non-bond energy plays an important role in the glass transition

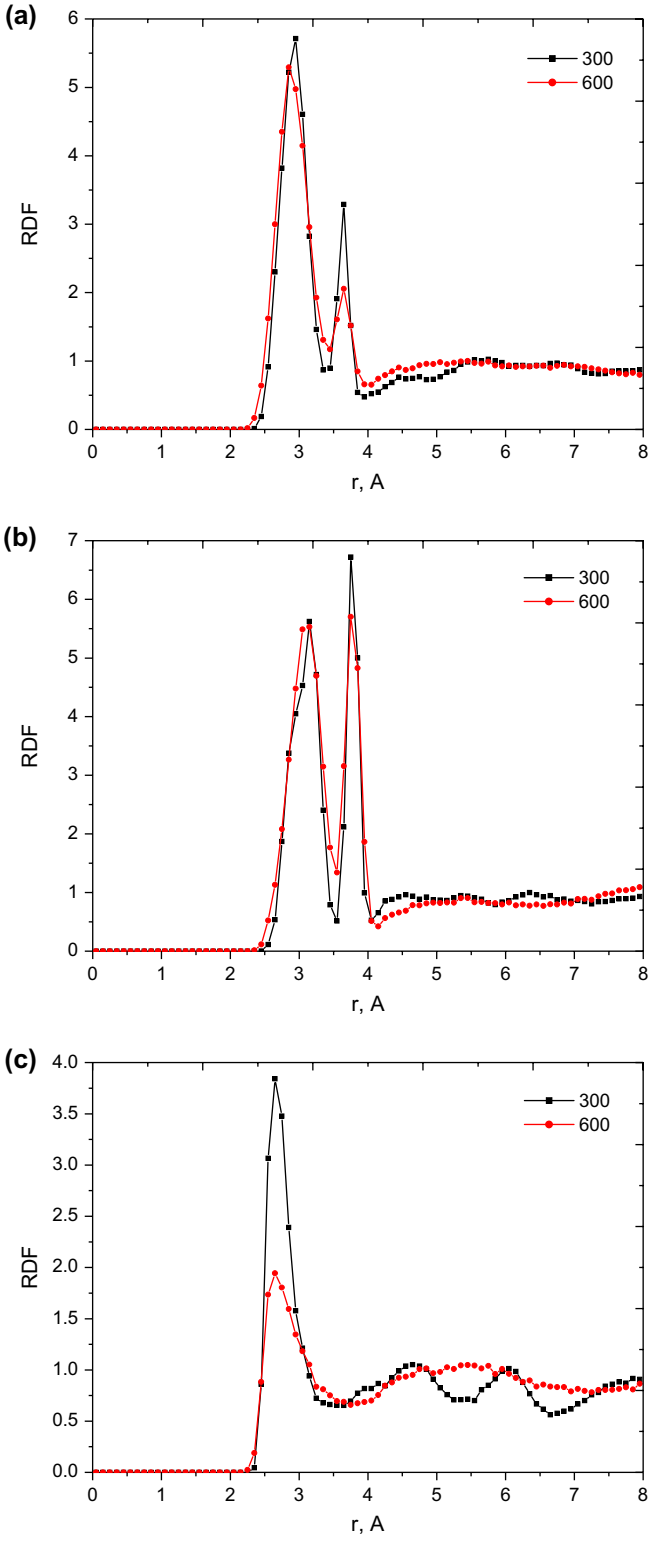

Fig. 4. The radial distribution functions (RDFs) for the three classes of polar atoms possible to form the hydrogen bonds: hydroxy oxygen–ether oxygen (a), hydroxy oxygen–nitrogen (b), and hydroxy oxygen–hydroxy oxygen (c).

process of the polymer system. However, we noticed that Li's group [38,39] performed the same analysis on PHB/PEO blend system [38] and POM system [39] and drew a different conclusion from ours: both torsion and non-bond energy played

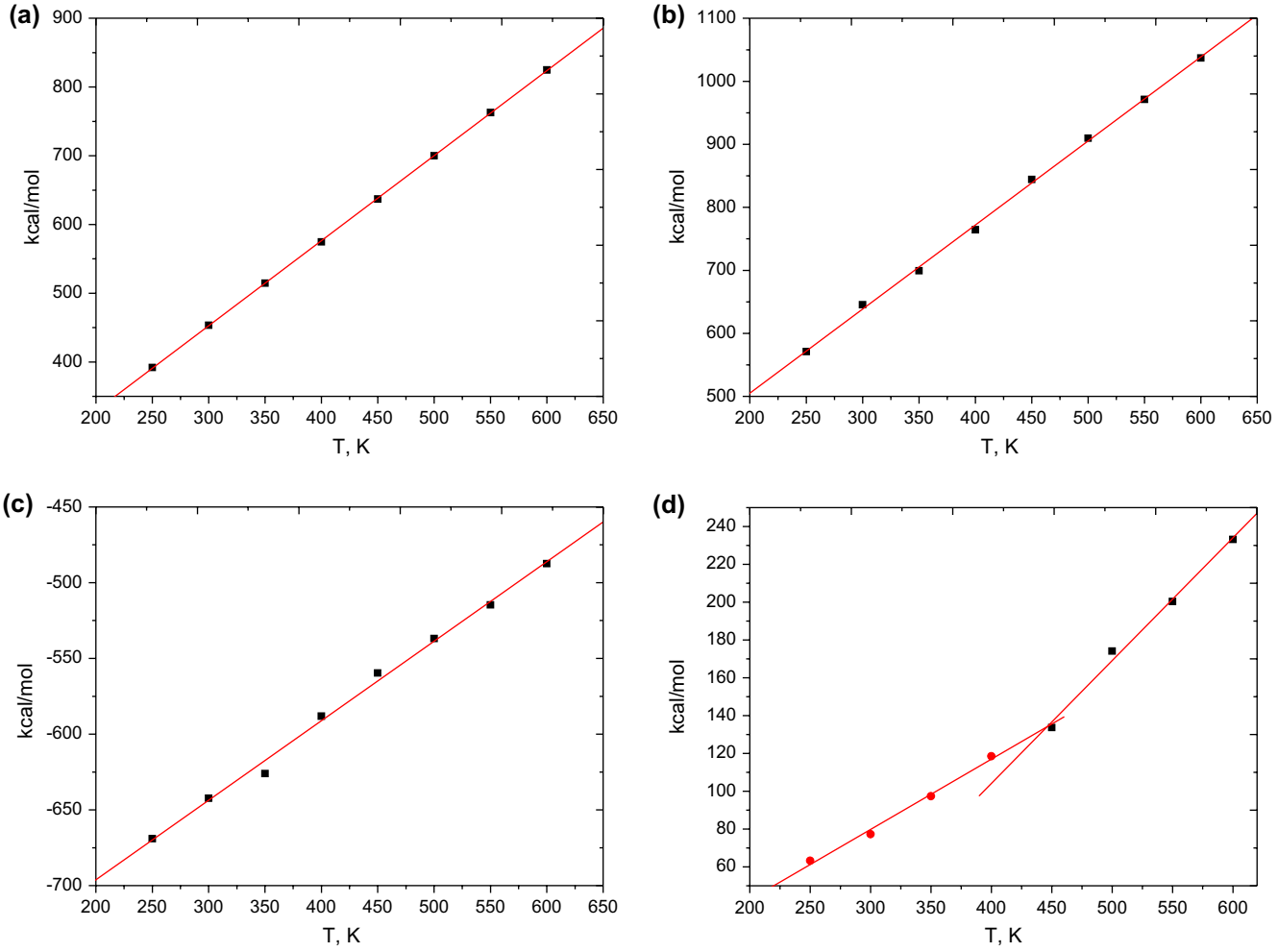

Fig. 5. Plots of some energy components versus temperature for the cured epoxy system: bond energy (a), angle energy (b), torsion energy (c), and non-bond energy (d).

important roles in glass transition. This difference can be associated with the fact that the torsions are significantly restricted in the polymer network.

The structural difference between glassy and rubbery states was further examined for this polymer system by calculating the torsion distributions of some typical segments. Four types of torsions (bonds 2, 3, 4, 5 as shown in Fig. 1) of epoxy segments between crosslinks were studied. These torsion angle distributions at 300 K and 600 K obtained as ensemble averages of all those types are shown in Fig. 6. Generally, these distribution functions exhibit same peak positions at the two different temperatures. For examples, the end (denoted by bond 2 in Fig. 1) and second (denoted by bond 3 in Fig. 1) torsion angles of epoxy segments are peaked around 0° (*trans*), +120° (*gauche*$^+$) and −120° (*gauche*$^-$); the fourth (denoted by bond 5 in Fig. 1) torsion angle connecting ether oxygen and phenyl carbon prefers the *trans* and *cis* conformations (−180° and +180°). Due to incomplete averaging, especially at low temperature [32], it is hard to draw a clear conclusion for the temperature dependence of these distribution functions. With a bit of exception, the torsion angle (denoted by bond 4 in Fig. 1) formed between methyl and ether represents only one favorable configuration (*trans*) at 600 K but three favorable configurations (0°, ±70°) at 300 K. This phenomenon that more structures are represented at lower temperature than at higher temperature is consistent with previous RDF results. The fourth torsion angle with better statistics seems to represent wider distribution at higher temperature than that at lower temperature as expected. It is worthwhile pointing out that the corresponding torsion angles of epoxy segments in a linear epoxy system represent populated conformations significantly different from these results reported here [40].

3.3. Dynamic properties

3.3.1. Translational dynamics of crosslinked nitrogen

The presence of crosslinks in the cured epoxy resins makes significant differences in structure and properties from the other linear polymers. It is instructive to analyze the motion of these crosslinks in the model systems as a function of temperature. Because of incomplete reaction, nitrogen atoms on the polymer chains can be classified as crosslinked and free ones. Generally, the crosslinked nitrogen atoms exhibit much lower mobility than the free nitrogen atoms due to topological

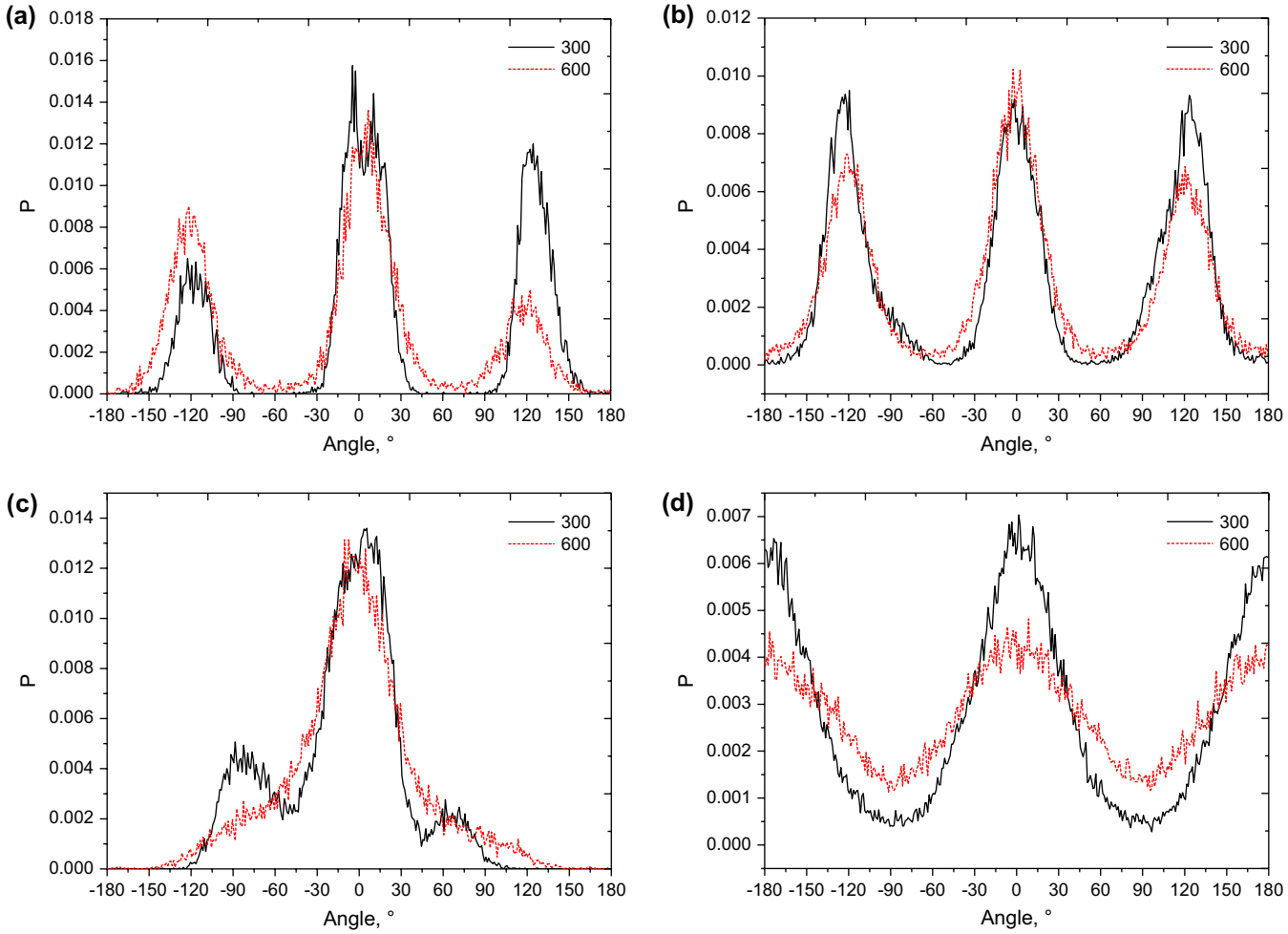

Fig. 6. The distributions for the end (a), the second (b), the third (c) and the fourth (d) torsion angles corresponding to positions 2, 3, 4, and 5 in Fig. 1, respectively, along the epoxy segments between the two crosslinks in the polymer network.

constraints. These differences can be characterized by calculating mean squared displacements (MSDs) according to the following relation

$$\mathrm{MSD} = \frac{1}{3N}\sum_{i=0}^{N-1}\left\langle |\vec{R}_i(t) - \vec{R}_i(0)|^2 \right\rangle \quad (2)$$

where R is the position of the atom, N is the total number of the atoms of a given type, and the broken brackets denote averaging over all choices of time origin.

The motion of those crosslinks can be expected to be quite different from that of the free Brownian particle where Einstein formula is valid [41]. Fig. 7 displays the temperature and time dependences of the MSD for the crosslinked nitrogen atoms. Only the first 100 ps out of 1000 ps was plotted because of two reasons: the motion was generally very slow and most movements were finished in the former several hundred picosecond interval; the short-time dynamics of the crosslinks was more accurate due to more time origins averaged (as shown in the Eq. (2)). The motion of crosslinked nitrogen atoms increases consistently with the increasing temperature (the diffusion behavior of uncrosslinked nitrogen atoms is anomalously temperature dependent due to poor statistics, which is not shown here). It is interestingly noted that mobility of crosslinked nitrogen atoms is distinctly different for lower temperatures (not higher than 400 K) and higher temperatures (not lower than 450 K). This abrupt change between the two temperature regions can be seen more clearly in Fig. 7(b), where the MSDs are replotted as a function of temperature at 10 ps long time. The change in the curve slope of MSD of segments versus T has been employed to identify the T_g of the general polymer surface [42], where the specific volumes are not defined and specific volume versus temperature cannot be used for the same purpose. Similarly, Tsige and Taylor used the constant-NVT ensemble dynamics procedure to locate the T_g of poly(methyl methacrylate) [43], where the model system was maintained at a constant volume at various temperatures. Differently, our work adopted realistic density values at the temperatures studied towards understanding molecular mechanism of glass transition. The translational behavior of crosslinks is similar to the averaged one of all atoms in the whole polymer segment although the former is about 3–4 times slower than the latter, as shown in Fig. 7(c). It is noted that uncrosslinked chains can affect the motion of crosslinked

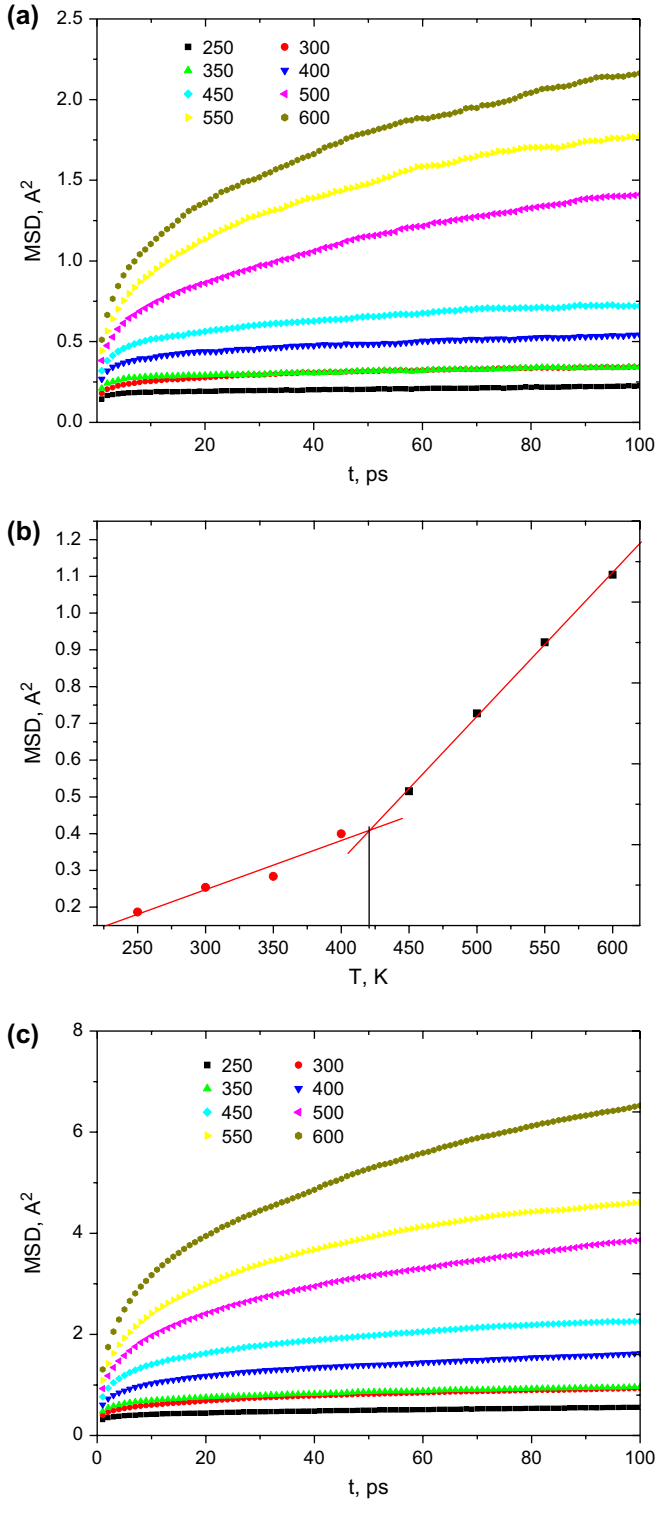

Fig. 7. Mean squared displacements (MSDs) of the crosslinks as a function of time (a) and temperature (b) for the epoxy polymer network system, MSDs of all atoms as a function of time are also shown in (c).

nitrogen atoms. However, these effects can be reduced when using larger size of system and higher conversion. Judging from these results, segment motions due to crosslinks can be related to the glass transition behavior of the whole polymer network. Specifically, it is highly desirable that the T_g of the polymer network with the full conversion can be obtained by short-time dynamics of the crosslinks with a lower conversion, such as MSD versus T.

Table 2
Description of bond vector codes in Figs. 8 and 9, referred to Fig. 1

Code	Description
1NC	Bond vector at position 1, connecting nitrogen atom with neighboring carbon along epoxy segment
2CC	Bond vector at position 2, connecting carbon atom with neighboring carbon along epoxy segment
3CC	Bond vector at position 3, connecting carbon atom with neighboring carbon along epoxy segment
4CO	Bond vector at position 4, connecting carbon atom with neighboring oxygen along epoxy segment
5OC	Bond vector at position 5, connecting oxygen atom with neighboring carbon along epoxy segment
6CC	Bond vector at position 6, connecting carbon atom with neighboring carbon along epoxy segment
12CH	Bond vector between positions 1 and 2, connecting bone carbon atoms with side hydrogen atom
23CH	Bond vector between positions 2 and 3, connecting bone carbon atoms with side hydrogen atom
34CH	Bond vector between positions 3 and 4, connecting bone carbon atoms with side hydrogen atom
56CH1	Bond vector 1 on phenyl group, connecting bone carbon atoms with side hydrogen atom
56CH2	Bond vector 2 on phenyl group, connecting bone carbon atoms with side hydrogen atom
23CO	Bond vector between positions 2 and 3, connecting bone carbon atoms with side oxygen atom
66′CC	Bond vector between positions 6 and 6′, connecting bone carbon atoms with side carbon atom

3.3.2. Rotational dynamics of chemical bond vectors

The value of T_g is well known to correlate closely to the chain flexibility. In molecular simulations, this flexibility can be conveniently quantified by vector autocorrelation functions (VACFs) of various bonds or segments along the polymer chain [24,25]. Some "backbone" and "side" bonds along the epoxy segments between crosslinks were studied here, whose notations are described in Table 2. Because of the anisotropy of the system, the second term, instead of the first term, of the Legendre polynomial is computed [44]:

$$P_2(t) = \frac{3\langle (u(t)\cdot u(0))^2 \rangle - 1}{2} \tag{3}$$

where $u(t)$ and $u(0)$ represent the unit vector at time t and time 0, respectively, and $\langle\ \rangle$ denotes the ensemble average over all such vectors and starting times.

Fig. 8(a) displays the evolution of these reorientation functions with time for some backbone bonds at the highest temperature (600 K). For the same two reasons noted above as for MSDs, only the first 100 ps is plotted in this figure. Additionally, due to more topology constraints, bond reorientation motion in polymer network perhaps shows more obvious anisotropy than that in linear polymers [45]. That first fast and then slow decrease in the vector orientation is observed from the crosslinks to middle phenyl rings. So the whole epoxy segments exhibit great diversity of dynamics. Similar results are

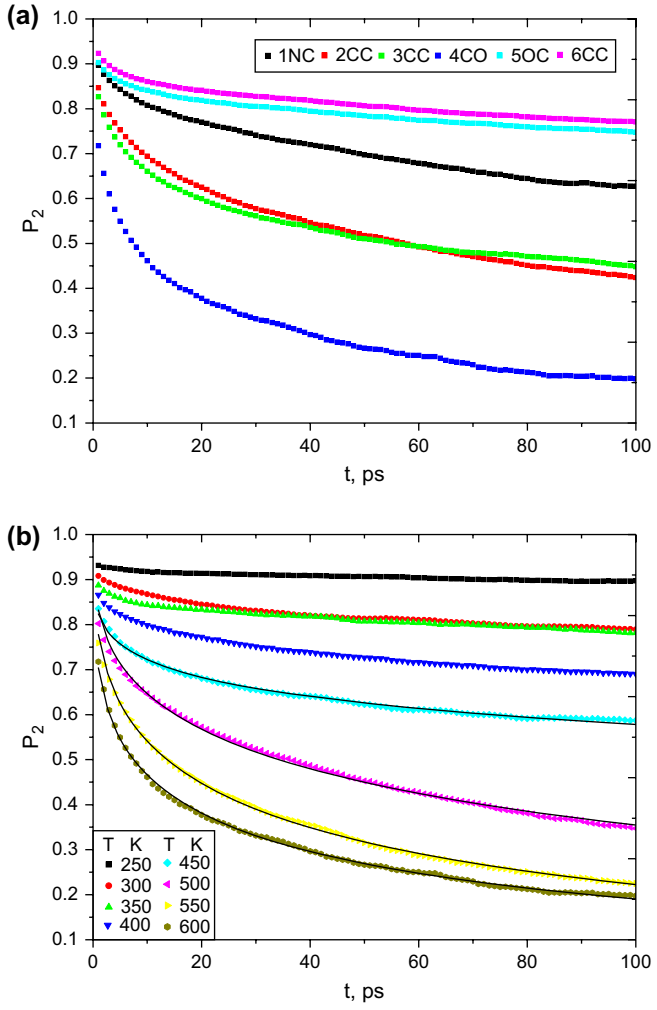

Fig. 8. The reorientation functions for some bonds along the epoxy segments as a function of simulation time at 600 K (a) and the fastest bond 4CO as a function of simulation time and temperature where black solid lines are KWW fitting at four higher temperatures (b). (For interpretation of the references to colour in this figure legend, the reader is referred to the web version of this article.)

applicable to other temperatures, but less clearly. It is noticed that the bonds 4CO (position 4 in Fig. 1) reorient the fastest among the studied backbone bonds. The reorientation function versus time of this fastest bond is plotted in Fig. 8(b) at various temperatures. This function increases with decreasing temperature at the same observation time interval, meaning that the chain segments are more mobile at higher temperatures. This behavior is in agreement with the general experimental observation. Further analysis indicates that these time-correlation functions of bond reorientation are not simple exponential ones but can be fitted well by the stretched exponential function, Kohlrausch–Williams–Watts (KWW) function [44,46]:

$$\phi(t) = \exp\left[-(t/\tau)^{\beta}\right] \tag{4}$$

where τ is the average relaxation time, and β is between 0 and 1 and represents the departure from a simple exponential

Table 3
The fitting parameters of KWW to the reorientation functions for the fastest backbone and side bonds at the four higher temperatures

Temperature, K	Backbone bond vector 4CO		Side bond vector 34CH	
	τ, ps	β	τ, ps	β
450	1454.5	0.225	1102.3	0.179
500	90.9	0.376	65.1	0.268
550	35.1	0.388	27.4	0.250
600	22.3	0.337	12.3	0.243

decay. This good fit has also been reported for backbone C–C bond vectors of the polyethylene liquids [45]. This is very true especially for the cases of higher temperatures. For the polymer network system studied here, the fitting parameters of the fastest backbone bond 4CO at the four higher

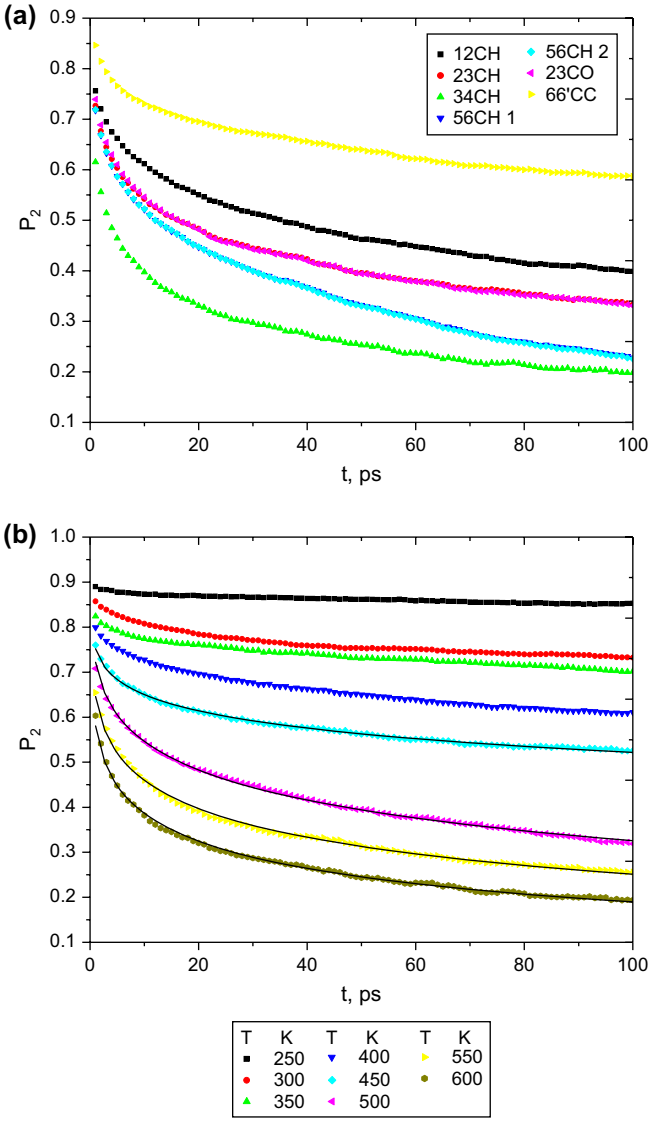

Fig. 9. The reorientation functions for some side bonds along the epoxy segments as a function of simulation time at 600 K (a) and the fastest bond 34CH as a function of simulation time and temperature where black solid lines are KWW fitting at four higher temperatures (b). (For interpretation of the references to colour in this figure legend, the reader is referred to the web version of this article.)

temperatures are shown in Table 3. Similar results were obtained for the side bonds attached to backbone atoms of epoxy segments, as shown in Fig. 9(a). The fastest bond vector is 34CH between positions 3 and 4, connecting backbone carbon atoms with side hydrogen atom, whose dependence of temperature is reported in Fig. 9(b) and the fitting parameters at four higher temperatures are also shown in Table 3. All the average relaxation times are found to increase with the decreasing temperature. Especially at 450 K, this parameter increases by almost one order of magnitude. This can also be associated with glass transition of the polymer system. Because of the limited simulation time employed in this work, these short-time dynamical results cannot apply to the Williams–Landel–Ferry (WLF) or Vogel–Fulcher–Tammann (VFT) equations occurring in glass transition [46].

4. Conclusions

Detailed MD simulations using COMPASS forcefield have been performed on a relatively simple polymer network model of a typical epoxy-amine system based on DGEBA and IPD. This model with highly crosslinked infinite network feature showed the difficulty in obtaining volumetric T_g by a general stepwise cooling constant-*NPT* MD procedure within the studied temperature range. But by adopting initial configurations appreciate for the experimental densities, constant-*NVT* MD simulations at the nanosecond scale can really reveal many interesting results on local structure and short-time dynamics associated with the crosslinks. The polymer system exhibits more structural features in case of below T_g than above T_g suggested by some typical radial distribution functions and torsion angle distributions. Specially, the calculated results of energy components and mean squared displacements (MSDs) also indicated the important roles of the non-bond energy (not torsion energy) and crosslinks in the glass transition of this polymer network system. A big great diversity was found in dynamics of polymer segments, and the reorientation functions can be well fitted by Kohlrausch–Williams–Watts (KWW) functions. A side result from these simulations is that to prepare the model system at the corresponding experimental density is very important to simulate (structure and dynamics of) a realistic polymer network. It is worth noting that 1 ns was long enough to obtain accurate relative results of local structure and short-time dynamics from the equilibrated initial configurations. According to our best knowledge, for the first time, these results have been reported for a polymer network. Because of the presence of the incomplete reactions, the effects of the uncrosslinked parts on the local structure and short-time dynamics of the simulated crosslinked parts reported in this work cannot be completely neglected. Further work is required in exploring these simulated results presented here using bigger size of system and higher conversion. Moreover, it is greatly desirable to compare these simulated results to the corresponding experimental data in the future.

Acknowledgements

Chaofu Wu wishes to acknowledge his wife, Wanhua Yang, and their parents who gave him continuous encouragement and supports in spirits and the Center of Molecular Simulation (situated at Hunan University) in Hunan province, which provides the computational platform (HP workstation and Materials Studio 4.0 package) for completing this work.

References

[1] Claybourn M, Reading M. J Appl Polym Sci 1992;44:565–75.
[2] Won Y-G, Galy J, Pascault J-P, Verdu J. J Polym Sci Part B Polym Phys 1991;29:981–7.
[3] Vallo CI, Frontini PM, Welliams RJJ. J Polym Sci Part B Polym Phys 1991;29:1503–11.
[4] Lesser AJ, Crawford E. J Appl Polym Sci 1997;66:387–95.
[5] Cheng K-C, Chiu W-Y. Macromolecules 1994;27:3406–14;
Cheng K-C, Lia KC, Chiu W-Y. J Appl Polym Sci 1999;71:721–8;
Chen Y-C, Chiu W-Y. Macromolecules 2000;33:6672–84;
Chen Y-C, Chiu W-Y. Polymer 2001;42:5439–48;
Cheng K-C, Don T-M, Rwei S-P, Li Y-C, Duann Y-F. J Polym Sci Part B Polym Phys 2002;40:1857–68.
[6] Hadicke E, Stutz H. J Appl Polym Sci 2002;85:929–35.
[7] Zhang Z, Yamashita T, Wong CP. Macromol Chem Phys 2005;206:869–77.
[8] Stevens MJ. Macromolecules 2001;34:1411–5;
Stevens MJ. Macromolecules 2001;34:2710–8;
Tsige M, Stevens MJ. Macromolecules 2004;37:630–7;
Tsige M, Lorenz CD, Stevens MJ. Macromolecules 2004;37:8466–72.
[9] Heine DR, Grest GS, Lorenz CD, Tsige M, Stevens MJ. Macromolecules 2004;37:3857–64.
[10] Wu C, Xu W. Polymer 2006;47:6004–9.
[11] Wang Q, Zhang X, Liu S, Gui H, Lai J, Liu Y, et al. Polymer 2005;46:10614–7.
[12] Watanabe O, Narita M, Ikawa T, Tsuchimori M. Polymer 2006;47:4742–9.
[13] Hu L, Frech R, Glatzhofer DT. Polymer 2006;47:2099–105.
[14] Yi JZ, Goh SH. Polymer 2005;46:9170–5.
[15] Wang YM, Ikeda A, Hori N, Takemura A, Ono H, Yamada T, et al. Polymer 2005;46:9793–802.
[16] Zheng W, Simon SL. Polymer 2006;47:3520–7.
[17] Subba Reddy CV, Sharma AK, Narasimha Rao VVR. Polymer 2006;47:1318–23.
[18] Baut NL, Diaz DD, Punna S, Finn MG, Brown HR. Polymer 2007;48:239–44.
[19] Sindt O, Perez J, Gerard JF. Polymer 1996;37:2989–97.
[20] Sun H. J Phys Chem B 1998;102:7338–64.
[21] Andersen HC. J Chem Phys 1980;72:2384–7.
[22] Berendsen HJC, Postma JPM, Van Cunsteren WF, Dinola A, Haak JR. J Chem Phys 1984;81:3684–90.
[23] Materials studio 4.0, visualizer, amorphous cell and discover modules. San Diego, CA: Accelrys Inc.; 2005
[24] Fried JR, Ren P. Comput Theor Polym Sci 1999;9:111–6;
Fried JR, Li B. Comput Theor Polym Sci 2001;11:273–81.
[25] Carbone P, Rapallo A, Ragazzi M, Tritto I, Ferro DR. Macromol Theory Simul 2006;15:457–68.
[26] Baselga J, Pozuelo J. Polymer 2002;43:6049–55.
[27] Abu-Sharkh BF. Comput Theor Polym Sci 2001;11:29–34.
[28] Ayulin AV, Balabaev NK, Michels MAJ. Macromolecules 2003;36:8574–5.
[29] Montserrat S, Calventus Y, Hutchinson JM. Polymer 2005;46:12181–9.
[30] Weyer S, Huth H, Schick C. Polymer 2005;46:12240–6.
[31] Leach AR. Molecular modeling principles and applications. London: Addison Wesley Longman Limited; 1996.
[32] Karayiannis NC, Mavrantzas VG, Theodorou DN. Macromolecules 2004;37:2978–95.

[33] Kang JW, Choi K, Jo WH, Hsu SL. Polymer 1998;26:7079–87.
[34] Barton JM, Deazle AS, Hamerton I, Howlin BJ, Jones JR. Polymer 1997;38:4305–10.
[35] Bennemann C, Paul W, Binder K, Dunweg B. Phys Rev E 1998;57:843–51.
[36] Soldera A. Polymer 2002;43:4269–75.
[37] Soldera A. Macromol Symp 1998;133:21–32.
[38] Yang H, Li Z-S, Qian H-J, Yang Y-B, Zhang X-B, Sun S-C. Polymer 2004;45:453–7.
[39] Yu K-Q, Li Z-S, Sun J. Macromol Theory Simul 2001;10:624–33.
[40] Barton JM, Buist GJ, Deazle AS, Hamerton I, Howlin BJ, Jones JR. Polymer 1994;35:4326–33.
[41] Lyulin AV, Michels AJ. Macromolecules 2002;35:1463–72.
[42] Morita H, Tanaka K, Kajiyama T, Nishi T, Doi M. Macromolecules 2006;39:6233–7.
[43] Tsige M, Taylor PL. Phys Rev E 2002;65:021805.
[44] Soldera A, Grohens Y. Polymer 2004;45:1307–11.
[45] Roe R-J. Adv Polym Sci 1994;116:111–44.
[46] Soldera A, Grohens Y. Macromolecules 2002;35:722–6.